Available online at www.sciencedirect.com
SCIENCE DIRECT®
Journal of Magnetic Resonance 172 (2005) 142–151
JMR Journal of Magnetic Resonance
www.elsevier.com/locate/jmr

SIMQUADNMR: a program for simulation and interpretation of multiple quantum-filtered NMR spectra of quadrupolar nuclei

Nicola D'Amelio, Elena Gaggelli, Elena Molteni[1], Gianni Valensin*

Department of Chemistry and the NMR Center, University of Siena, Via A.Moro, 53100 Siena, Italy

Received 17 June 2004; revised 28 September 2004

Abstract

In this paper, we present a computer program which simulates NMR multiple quantum-filtered spectra of quadrupolar nuclei as a function of physical parameters, of the type of experiment and experimental conditions. The program works by solving relaxation theory equations for the given system, and it can be useful in order to plan the ideal conditions to set up specific experiments or to give a physical interpretation of experimental results. The program allows to independently follow the dependence of individual coherences and relaxation rates as a function of up to 50 parameters regarding the physical properties of the system under investigation, sample conditions and instrumental setup making it an helpful tool also for teaching purposes.

Keywords: Quadrupolar; NMR; Computer program; Simulation; Multiple quantum-filtered spectra

1. Introduction

Although around two-thirds of nuclei usually quoted in NMR tables have spin $I > 1/2$, the vast majority of studies have been limited to the relatively few $I = 1/2$ nuclei. As a consequence, most theoretical and experimental advances have focused on improving the performance of NMR investigations of ^{1}H, ^{13}C, ^{15}N, ^{31}P, ^{29}Si of progressively larger molecules in solution or in the solid state.

However, the interest in some $I > 1/2$ nuclei (especially form the biological point of view), such as ^{2}H, ^{17}O, ^{23}Na, ^{25}Mg, ^{33}S, ^{35}Cl, ^{39}K, ^{43}Ca, has attracted several investigators who provided many ways of facing the intrinsic complexity of such NMR studies [1–4]. In fact, the non-spherically symmetric electrical charge distribution within $I > 1/2$ nuclei gives rise to a nuclear electrical quadrupole moment, which interacts with electric field gradients, producing splittings of the nuclear energy levels.

Therefore, the interpretation of NMR data for the study of the atomic properties of systems containing quadrupolar nuclei, although potentially highly informative due to the large number of parameters involved in both the observed shifts and relaxation rates, is generally hindered by the complexity of the equations describing these phenomena. These equations are especially cumbersome in case of nuclei with high nuclear spin quantum number because of the increased number of atomic levels and therefore possible transitions.

A tool for interpreting the experimental spectra in terms of physical parameters (e.g., viscosity of the solution, charge distribution symmetry around the nucleus, molecular weight of the system) and the effects of pulses and delays could be useful for unraveling the chemical processes under investigation.

The presence of slow motions on the NMR time scale (that is when the system is outside the extreme narrowing limit) allows the detection of multiple-quantum

* Corresponding author. Fax: +39 0577 234254.
E-mail address: valensin@unisi.it (G. Valensin).
[1] Her work was supported by CIRMMP (Consorzio Interuniversitario Risonanze Magnetiche di Metalloproteine Paramagnetiche).

1090-7807/$ - see front matter © 2004 Elsevier Inc. All rights reserved.
doi:10.1016/j.jmr.2004.10.005

coherences which can be originated by the non-monoexponentiality of the relaxation rates or in cases of partially oriented systems. Such coherences are in some cases narrower than the corresponding single-quantum coherence and can be used for a variety of applications. For example, multiple quantum filtered (MQF), and in particular triple quantum-filtered (TQF) experiments have been extensively used to reduce the large signal due to extracellular ^{23}Na seen in single quantum (SQ) spectra [5,6]. Some contribution from extracellular ^{23}Na is present in the observed signal, but it can be identified by using shift reagents acting outside the cell membrane [6]. Another application has been found for ^{2}H which gives rise to double quantum (DQ) coherences in the presence of residual quadrupolar interaction. By filtering the large quantity of isotropic tumbling heavy water, it is possible to select water interacting with biological fibers such as tendons and use the signal for creating images in a non-invasive fashion [7].

In this paper, we present a useful tool to interpret NMR data on quadrupolar nuclei. SIMQUADNMR is a program which simulates NMR MQF spectra of quadrupolar nuclei based on the physical parameters of the system (motional correlation time, exchange rates, etc.) and on the experimental conditions (magnetic field, pulses, and delays). The program can be used for estimating the possibility to run one kind of experiment (and in case optimize the experimental parameters) or for interpreting from a physical point of view the experimental spectra.

2. Algorithm

The program solves the evolution of the density matrix (expressed in a appropriate tensor basis) describing a quadrupolar nucleus under the effect of hard pulses (rotation matrices) and of the hamiltonian acting during delays (Liouville–von Neumann differential equation) of a multiple quantum filtering pulse sequence.

Nuclei with spin larger than 1/2 have a non-vanishing electric quadrupole moment, due to their asymmetric charge distribution. The quadrupole moment can interact with local oscillating electric field gradients, due to electrons, and this is almost always the main relaxation mechanism in solution [8,9].

The quantum-mechanical expression for the quadrupole Hamiltonian is

$$H_1(t) = \frac{e^2qQ}{4\hbar I(2I-1)}\left\{3I_z^2 - I(I+1) + \tfrac{1}{2}\eta(I_+^2 + I_-^2)\right\}, \tag{1}$$

where I is the nuclear spin quantum number, eq is the main component of the diagonalized tensor describing the second derivative of the electric potential (q is called the quadrupolar factor), eQ is the nuclear quadrupolar constant, and η is the asymmetry parameter ($0 \leqslant \eta \leqslant 1$; $\eta = 0$ in case of axial symmetry of the nuclear surroundings). The quantity $e^2qQ/\hbar$ is called the quadrupole coupling constant and it measures the magnitude of the nuclear quadrupolar interaction.

2.1. Spin tensors basis

Solving the evolution for a time-dependent Hamiltonian requires to expand the density matrix in an appropriate orthonormal spin basis of dimension $(2I+1)^2$ [10,11]. We decided to use two possible bases $\{B_r\}$.

(1) The spherical spin tensors basis [12]. This has the advantage of containing tensors directly related to observables: for example, I_z is related to equilibrium magnetization while I^+ (or I^-) is related to the observable signal.

(2) The coherences basis: this basis has one element different from zero in every basis matrix and represents populations and coherences (1-quantum to n-quantum going far from the diagonal) of the system. This basis is useful to get insight into the physical properties of the system (for example the effect of the correlation time on each transition).

In both bases, each element is identified by two indexes q and k. In particular, q describes q-quantum transitions between levels and can be either positive (for jumps from bottom to top energies) or negative (from top to bottom); k distinguishes between different q-quantum transitions in the system (for example in ^{23}Na three different single-quantum transitions are possible). In addition, k can range from 0 to the rank of the matrix ($2I$) while q ranges from $-k$ to k; the rank of the matrix indicates the maximum transition possible in the system (for ^{2}H the highest transition is the double-quantum).

2.2. Relaxation and frequency matrices

The calculation of the evolution of σ (density matrix) during the delays of the pulse sequence, requires an evaluation of the frequency and relaxation matrices, Ω and Γ, defined as [10]:

$$\Omega_{r,s} = \langle B_r|[H_0, B_s]\rangle / \langle B_r|B_r\rangle \tag{2}$$

and

$$\begin{aligned}\Gamma_{r,s} &= \langle B_r|\hat{\Gamma}B_s\rangle / \langle B_r|B_r\rangle \\ &= \frac{1}{2}\sum_q \sum_p \left\{\langle B_r|[A_{k,p'}^{-q}, [A_{k,p'}^{q}, B_s]]\rangle / \langle B_r|B_r\rangle\right\}(-1)^q j(p\omega),\end{aligned} \tag{3}$$

where $j(p\omega)$ are the spectral density functions (vide infra), $B_{r,s}$ are two elements of the tensor basis used to describe the density matrix and $A_{k,p}^{q}$ are tensor spin

operators used for the decomposition of the quadrupolar Hamiltonian H_1 [13]:

$$\begin{aligned}
A^0_{2,0}(i,j) &= \{2I^2_z(i,j) - \tfrac{1}{2}[(I_+I_-)(i,j) + (I_-I_+)(i,j)]\},\\
A^1_{2,1}(i,j) &= \tfrac{\sqrt{6}}{2}[(I_+I_z)(i,j) + (I_zI_+)(i,j)],\\
A^{-1}_{2,1}(i,j) &= \tfrac{\sqrt{6}}{2}[(I_-I_z)(i,j) + (I_zI_-)(i,j)],\\
A^2_{2,2}(i,j) &= \tfrac{\sqrt{6}}{2}I^2_+(i,j),\\
A^{-2}_{2,2}(i,j) &= \tfrac{\sqrt{6}}{2}I^2_-(i,j),
\end{aligned} \tag{4}$$

where i and j indexes indicate rows and columns.

It should be noticed that our description does not include interactions other than quadrupolar (e.g., dipolar or chemical shift anisotropy) although in some cases cross-correlation with other mechanisms may be relevant even when the quadrupolar interaction is the main relaxation mechanism [14]. Comparison with experimental data may reveal such cases.

The case of systems where the motion is locally anisotropic is considered in H_0, which is defined as [8,9]:

$$H_0 = \Delta\omega I_z + \omega_q\left[3I^2_z - I^2 + \eta\left(I^2_x - I^2_y\right)\right] \tag{5}$$

with

$$\omega_q = f\frac{eQ}{4\hbar I(2I-1)}V_{zz} \tag{6}$$

and

$$V_{zz} = eq\left[\cos^2\theta - \frac{1}{2}\sin^2\theta + \frac{1}{2}\eta\sin^2\theta\cos(2\varphi)\right], \tag{7}$$

where $\Delta\omega = \omega_0 - \omega$ is the offset of the RF carrier frequency ω from the resonance frequency ω_0, f is a scaling factor reducing the quadrupolar coupling to the residual one ω_q due to fast exchange with isotropic states where the quadrupolar interaction averages to zero, θ and ϕ define the orientation of the electric field gradient tensor with respect to the static field, η is the asymmetry parameter, V_{zz} is the z component (the largest) of the electric field gradient and eQ is the nuclear quadrupolar constant. In the presence of a distribution of sites with different local orientation and residual quadrupolar coupling, the global spectrum can be reconstructed by adding a series of spectra obtained by simultaneously varying both parameters with a distribution of values which best reproduces their probability. The present description implies fast exchange between isotropic and locally anisotropic sites and slow exchange among anisotropic sites.

To calculate the spectral densities, three models of motion were considered: sphere, prolate ellipsoid, and oblate ellipsoid. In the program the rotational diffusion coefficients $D_\perp$ and $D_\parallel$ can be given in input or calculated (clicking on the *motion* button) based on the size of the molecule, the hydration radius, the viscosity and the chosen model; the molecule size, if unknown, can be estimated based on the molecular weight given the axial ratio and assuming a specific volume of 0.73 $cm^3\ g^{-1}$. The equations used to calculate $D_\perp$ and $D_\parallel$ as a function of molecule size, for the three models, are reported elsewhere [15].

Once the rotational diffusion coefficients were determined, the spectral densities were calculated for the isotropic and anisotropic case as follows [16]:

(a) isotropic

$$J(p\omega) = \frac{2}{5}\frac{e^2qQ}{4\hbar I(2I-1)}\left(1 - \frac{1}{3}\eta\right)\left(\frac{\tau_c}{1 + (p\omega\tau_c)^2}\right), \tag{8}$$

where τ_c is given by

$$\frac{1}{\tau_c} = 6D_\perp, \tag{9}$$

(b) anisotropic

$$\begin{aligned}
J(p\omega) = \frac{2}{5}\frac{e^2qQ}{4\hbar I(2I-1)}
&\times\left\{\left[3\cos^2\alpha - 1 - \eta\sin^2\alpha\cos(2\beta)\right]^2\left(\frac{\tau_{c0}}{1 + (p\omega\tau_{c0})^2}\right)\right.\\
&+\left[12\sin^2\alpha\left(\cos^2\alpha(1 + 2\eta\cos(2\beta)) + \left(\frac{1}{3}\eta\right)^2\right.\right.\\
&\times\left.\left.\left(1 - \cos^2(2\beta)\sin^2\alpha\right)\right)\left(\frac{\tau_{c1}}{1 + (p\omega\tau_{c1})^2}\right)\right]\\
&+\left[3\sin^4\alpha - 2\eta\sin^2\alpha(\cos^2\alpha + 1)\cos(2\beta)\right.\\
&\left.\left.+\frac{1}{3}\eta^2(\cos^2(2\beta)\sin^4\alpha + 4\cos^2\alpha)\right]\left(\frac{\tau_{c2}}{1 + (p\omega\tau_{c2})^2}\right)\right\},
\end{aligned} \tag{10}$$

where $\tau_{cm\,=\,0,1,2}$ is given by:

$$\frac{1}{\tau_{cm}} = 6D_\perp + m^2(D_\parallel - D_\perp) \tag{11}$$

and α and β are the angles defining the orientation of the electric field gradient tensor with respect to the rotational diffusion tensor (considered axially symmetric). α is the angle between the z axis of the electric field tensor and the z axis of the diffusion tensor, β defines the remaining orientation.

Multiplication by $n\omega\tau$ is used to obtain the imaginary part of the spectral density function, leading to second order frequency shifts of the resonance lines, which are called dynamic frequency shifts (DFS) and can be included in the frequency matrix [17].

During the calculation the program checks for Redfield limit violation and warns the user when the correlation time modulating the quadrupolar interaction is larger than 1/100 (Redfield limit approaching) or 1/10 (Redfield limit violated) of the inverse of the relaxation matrix element.

In addition, the exchange rates are included in the relaxation matrix. The program allows up to three sites. Each site enlarges all matrices adding rows and columns to the dimension of the original one-site matrix. On the other hand, only few elements have to be calculated:

$$K_{mn} = k_{nm\,(m\neq n)} \tag{12}$$

and

$$K_{mm} = -\sum_{\substack{n=1\\ n\neq m}} k_{mn}, \tag{13}$$

where K_{mn} is the matrix element connecting corresponding coherences in different species involved in the equilibrium and k_{mn} are the rate constants for the conversion of the species m into the species n [10]. The concentrations of the various species at equilibrium can be calculated by clicking on the *calculate equilibrium conc* button, if the analytical concentrations and the equilibrium constant are known. The program accounts for three models of exchange phenomena based on different kinds of equilibrium:

(1) $Q_1 \leftrightarrows Q_2$
(2) $Q_1 + b\mathrm{B} \leftrightarrows Q_2$ for which k_{on} is replaced by $k_{on}[\mathrm{B}]^b$
(3) $Q_1 + b\mathrm{B} \leftrightarrows Q_2 + c\mathrm{C}$ for which k_{on} is replaced by $k_{on}[\mathrm{B}]^b$ and k_{off} by $k_{off}[\mathrm{C}]^c$.

In the equations Q indicates the species containing the quadrupolar nucleus and B, C are generic interacting molecules.

2.3. Building the propagator

As in the case of the rotation matrix for the evolution during pulses, the operator $\exp((-\Gamma - i\Omega)t)$ has to be applied to the density matrix for the evolution during delays. Using the Taylor expansion may require in this case a long computational time besides overflow of the computer; in fact, due to the high numbers appearing in the relaxation and frequency matrices for such systems, especially in slow motion regime, the expansion may require many terms to reduce the error.

To overcome this problem, we used a modified version of the Taylor expansion, the "scaling and squaring" method [18, and references therein]: the idea is to choose m to be a power of two for which $e^{A/m}$ can be reliably and efficiently computed, and then to form the matrix $(e^{A/m})^m$ by repeated squaring.

2.4. The pulse sequence

Once the evolution under the effect of the pulses and during the delays is defined, the equilibrium density matrix is let to evolve under the effect of the MQF pulse sequence whose basic scheme is 90°–$\Delta/2$–180°–$\Delta/2$–90°–t_1–90° [19–24]. In this experiment, multiple-quantum coherences are created, selected, and transformed into observable magnetization. The program allows the introduction of an extra pulse and delay besides giving the possibility of choosing the phase of the pulses (x or y) although the effect of spin lock is not herein considered. The phase cycling used for coherence selection is simulated by filtering the density matrix after t_1 evolution that is, in case of a q-quantum filter, by extracting terms which are q elements distant from the main diagonal. During each delay the density matrix is expanded into the chosen basis set, the propagator is built according to the evolution time and applied to the coefficients of the expansion. Then, the density matrix is reconstructed using the new coefficients. During the acquisition time, the propagator corresponding to the dwell time is built and used for all points of the FID. Each point of the FID has an imaginary and a real part, which are obtained by taking the trace of the products between the imaginary and real parts of the density matrix with the operator I^+, which represents the observable magnetization. The Fourier transform finally generates the spectrum in the range of frequencies chosen.

2.5. Calculating the q factor

The quadrupolar q factor depends on the second derivative of the potential $\partial^2 V/\partial z^2$ ($V_{zz} := eq := \partial^2 V/\partial z^2$), which arises from the presence of external charges (nuclei or electrons) in the neighborhoods of the quadrupolar nucleus under examination.

Given the geometry of the molecule in Cartesian coordinates, the components of the tensor describing the second derivative of the potential are calculated as follows [9]:

$$V_{\alpha\beta} = \frac{\partial^2 V}{\partial\alpha\partial\beta} = \frac{1}{4\pi\varepsilon_0}\frac{e}{r^3}\left(\frac{3x_\alpha x_\beta}{r^2} - \delta_{\alpha\beta}\right) \tag{14}$$

with $\alpha, \beta = x, y, z$.

Once the tensor has been calculated, it is diagonalized using the Jacobi method to align the principal axes of the tensor with the Cartesian axes. Finally, the z component is by definition the largest among the three and the q factor is calculated as $q = (\partial^2 V/\partial z^2)/e$ while the asymmetry parameter is calculated as $\eta = |V_{xx} - V_{yy}|/V_{zz}$.

The geometry of the molecule can be provided also in spherical coordinates which are then transformed by the program into Cartesian to use the same algorithm.

This calculation takes into account only neighboring atoms and their charges and is therefore valid only for closed shell quadrupolar nuclei (where the electronic charge is spherically symmetric and thus does not contribute to quadrupolar coupling). It is important to underline that the calculation does not take into account the Sternheimer factor $\gamma(r)$ [9] which accounts for distortion of the spherical symmetry of the electronic charge

due to the presence of an external charge. This factor leads to a correction of q such that $q = q^0[1 - \gamma(r)]$, where q^0 is the theoretical value neglecting this effect. This factor, although negligible for open shell nuclei, may affect by one or two orders of magnitude the calculated value of q provided the charge dwells outside the closed shell charge distribution. In this case, the factor becomes independent of the distance from the nucleus r and quite sizable. On the contrary, when the charge is well inside the closed shell, the Sternheimer factor is dependent on the distance r and in general $\ll 1$ making the correct estimation of the q factor possible.

2.6. Write equation routine

From a theoretical point of view, the analytical form of the evolution of the various coherences describing the system may be useful to understand the effect of relaxation. The equations for the evolution of each tensor describing different parts of the global density operator (that is the magnetization) constitute a system of interdependent differential equations in which each variable (operator) is multiplied by a factor which in turn is a linear combination of the spectral densities at zero frequency, Larmor frequency and twice the Larmor frequency. To write the equations, the coefficients of the linear combinations of the spectral densities have to be determined and this is done by solving Eq. (3) without the summation over the p index.

Running this routine in the coherences basis allows to get insight into the evolution of each transition; the routine in fact translates the names of the operators into populations and transitions between levels (the conversion is shown in a legend). When using the spherical spin tensors basis, only few equations have a direct physical meaning, the ones involving the operators I_z, I^+ or I^-. To get insight into the other tensors, a legend is made in this case that translates each spherical spin tensor in terms of common operators as products of I_z, I^+, I^-, I^2, and their powers. In other words, the legend is built by expanding the spherical spin tensors into this new basis which, on the other hand, is not orthogonal. As a consequence the legend can only state the presence of a contribution from each one of the common operators, but cannot say how large this contribution is, unless only one common operator can alone describe the spherical spin tensor under examination. For example, in the case of $I = 3/2$, the spherical spin tensor with $q = 0$ and $k = 1$ is exactly $-0.448 I_z$, while the spherical spin tensor with $q = 1$ and $k = 2$ contains $I_z I^+$ but also other terms.

2.7. Plotting matrices

The program allows visualization of the main matrices calculated in the spin tensor basis used. These include relaxation and exchange matrix, the frequency matrix (including dynamic frequency shifts), the propagator at a time t (that is the exponential form of the relaxation, exchange and frequency matrices), the rotation matrix with its inverse for a given angle, rank 2 matrices describing the Hamiltonian for the quadrupolar interaction (the ones called $A^q_{k,p}$ in Eq. (4)), all matrices constituting the spin tensors basis, some common matrices like I_x, I_y, I^-,... for a given I and the density matrix at every stage of the pulse sequence.

This option may be a useful tool to get insight into the physics of the experiment.

2.8. Plotting graphs

Making graphs of some properties of the spectrum is a useful tool to optimize experimental parameters or to derive physical parameters of the system under examination by comparing simulation with experimental data. The program gives the possibility of plotting many spectra one upon each other or in a 3D fashion and also to plot the following properties:

- relaxation rates,
- cross-relaxation terms between coherences,
- coherences,
- peak height,
- linewidth,
- dynamic frequency shifts,

as a function of the following parameters (in logarithmic or linear increment):

Experimental

- the nucleus (spectra of different nuclei can be compared and the different nuclei are chosen in the box named "*periodic table*"; choosing the nucleus automatically sets I, Q, γ, natural abundance, but each of these parameters can also be varied independently, as explained below);
- temperature, T;
- sample concentration;
- active volume;
- magnetic field strength (expressed as proton frequency frq_prot);
- delays of the pulse sequence (t_1, Δ);
- rotation angle of each pulse;
- phase of each pulse;
- kind of filter;
- acquisition time;
- number of points for sampling the FID, TD;
- line broadening LB;
- number of scans NS;
- noise level;
- angles for phasing the spectrum at order zero and at first order, and position of the cursor;

- right (sw1) and left (sw2) limits of the spectral width;
- number of points for the Fourier transform, SI.

Physical

- correlation time modulating the quadrupolar interaction τ_c;
- rotational diffusion coefficients $D_\perp$ and $D_\parallel$;
- nuclear quantum number I;
- nuclear quadrupolar constant Q;
- gyromagnetic ratio γ;
- percentage natural abundance of the selected isotope;
- frequency of the chosen nucleus at the given magnetic field, ω;
- offset from the transmitter $\Delta\nu$;
- quadrupolar q factor measuring the size of the gradient of the electric field generated by the ligands;
- asymmetry parameter η;
- angles of the electric field gradient tensor with respect to the rotational diffusion tensor, α and β;
- scaling factor f reducing the magnitude of the quadrupolar interaction to the residual one;
- angles θ and ϕ formed by the molecular local symmetry axis with the external magnetic field in partially oriented systems;
- residual quadrupolar interaction ω_q present in partially oriented systems;
- exchange rates k_{on}, k_{off};
- molar fraction of each site;
- concentrations of the various species present (in case of exchange).

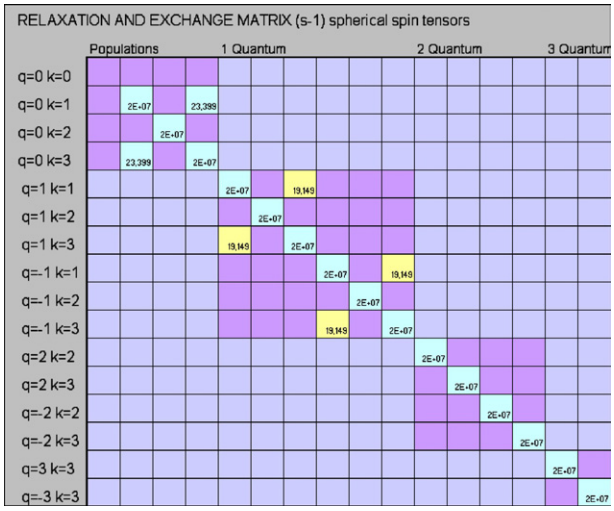

Fig. 1. Relaxation matrix of ^{23}Na in the basis of spherical spin tensors. Observable magnetization (represented by the tensor with $q = 1$ and $k = 1$) has a cross-term (yellow) with the tensor identified by $q = 1$, $k = 3$. This cross-term can transform single quantum transitions (generated by the first 90° pulse) into triple quantum transitions (generated by the third rank tensor after the effect of the second 90° pulse). Assumed parameters are those reported in the caption of Fig. 4 for the bound form.

Each property can be plotted as a function of one or two variables (2D or 3D graph). Alternatively, one property which is constituted by more elements (e.g., all the coherences) can be plotted as a function of one variable generating a 3D graph. In such cases, it is sometimes useful to filter out elements which are not of interest. For example, when monitoring relaxation rates one may be interested in following only single-quantum coherences or one cross-relaxation term.

Finally, one can choose to monitor the imaginary or real part of any coherence at each stage of the pulse sequence to optimize delays and pulses.

2.9. Example, the case of ^{23}Na in biological systems

As a case example we will reproduce the spectrum of Na^+ ion interacting with a locally anisotropic system (e.g., cartilage).

Due to the spin number $I = 3/2$ the system can be described with tensors up to the third rank. It has been

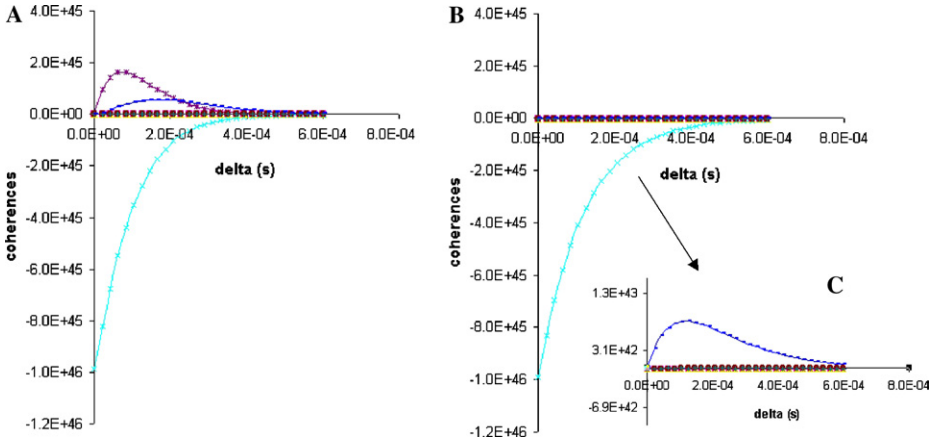

Fig. 2. Contribution of T_{11} (cyan), T_{12} (magenta), and T_{13} (blue) to the density matrix after the delay Δ of the pulse sequence (Eq. (15)) for an aligned (A) and isotropic (B) system. (C) y scale magnification of (B). The delay Δ was varied between 1 μs and 0.6 ms. (For assumed microscopic parameters see those reported in the caption of Fig. 4 for the bound form.)

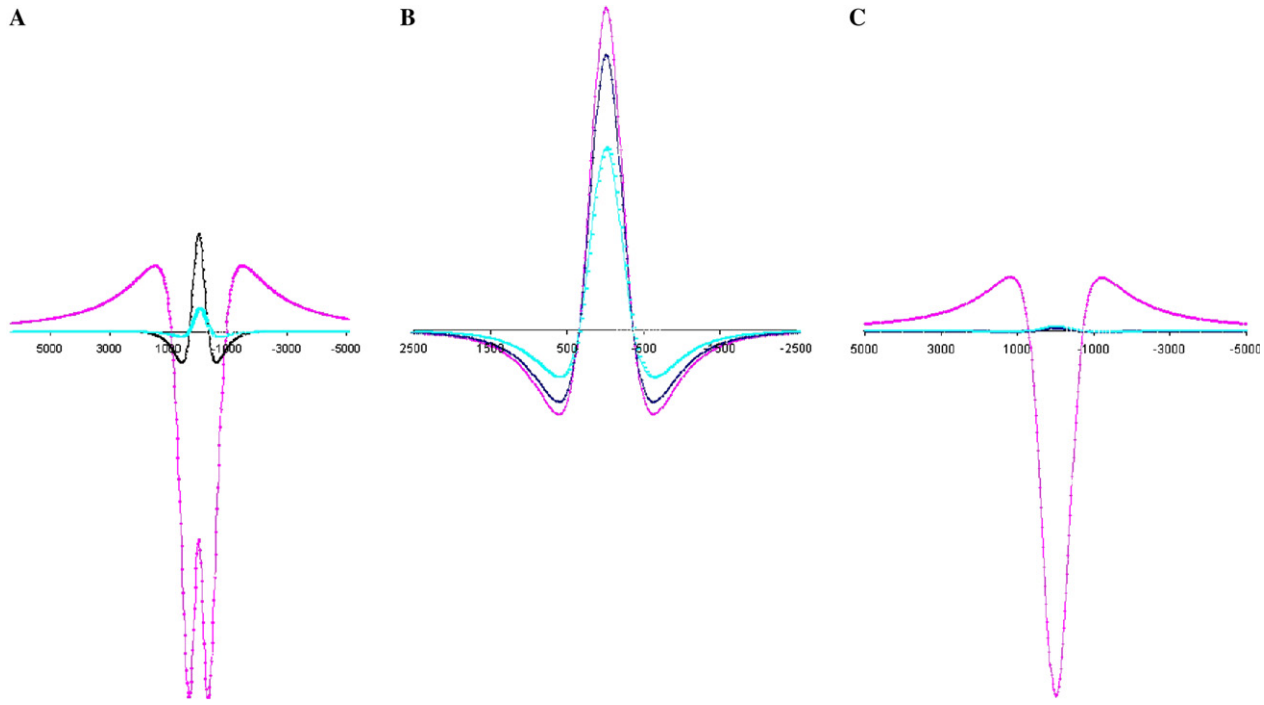

Fig. 3. DQF (A,C) and TQF (B) simulated spectra of Na^+ interacting with cartilage. All parameters were chosen to reproduce data reported in [25]. Pulse sequence parameters are $\Delta = 1.0$ ms (magenta), 1.6 ms (blue), 2.2 ms (cyan); $t_1 = 30$ μs, $\varepsilon = 90°$ (A,B) and 54.73° (C). Assumed microscopic parameters for the bound Na^+: isotropic motion with a rotational diffusion value of 1.85×10^8 s^{-1} (equivalent to a sphere tumbling with a rotational correlation time of 0.9×10^{-9} s), axial electric field with $q = 3.97 \times 10^{39}$ J m^{-2} C^{-2} (resulting in a quadrupolar coupling e^2qQ/h of 0.6 MHz), a residual quadrupolar coupling due to partial orientation with respect to the magnetic field of 10 kHz (obtained by a proper combination of the scaling factor and the orientation angle θ). Assumed microscopic parameters for the free Na^+: isotropic motion with a rotational diffusion value of 8.33×10^9 s^{-1} (equivalent to a sphere tumbling with a rotational correlation time of 2×10^{-11} s), axial electric field with $q = 1.53 \times 10^{39}$ J m^{-2} C^{-2} (resulting in a quadrupolar coupling e^2qQ/h of 1.55 MHz), no residual quadrupolar coupling. The exchange between these two sites was described by using the kinetics constants $k = 1 \times 10^7$ s^{-1} and $k^{-1} = 2.2 \times 10^7$ s^{-1} where the "on" reaction describes the conversion from free to bound sodium. In all cases a field was chosen at which ^{23}Na resonates at 52.9 MHz. Other parameters $T = 298$ K, molar fraction of the bound form = 0.018.

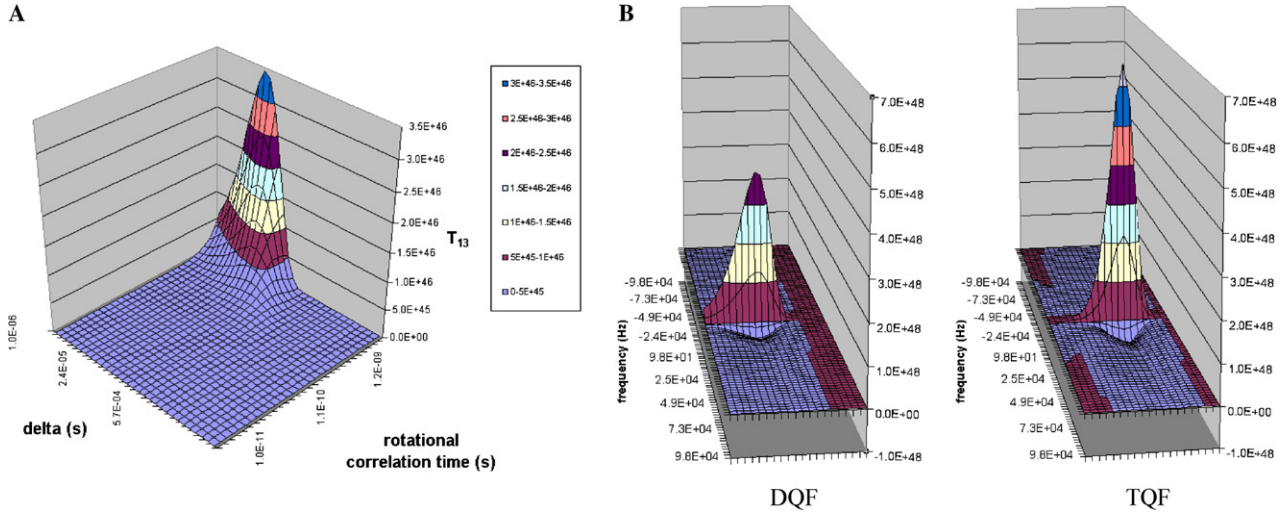

Fig. 4. (A) Quantification of T_{13} tensor contribution to the density matrix after the delay Δ of the pulse sequence (Eq. (15)) as a function of the motional correlation time and Δ value. (B) DQF and TQF simulated spectra of Na^+ interacting with a large protein (e.g., bovine serum albumin) as a function of the delay Δ ranging from 1 μs (left) to 3 ms (right). All parameters are those reported in the caption of Fig. 3 except the rotational diffusion of the bound form (9.31×10^6 s^{-1}). The rotational diffusion was estimated through Stokes–Einstein law by the molecular weight of the interacting protein (68 kDa), the viscosity of water at 298 K (8.938×10^{-4} kg m^{-1} s^{-1}) assuming a hydration radius of 0.27 nm (corresponding to a value in-between half and one hydration sphere) and a specific volume of 0.73 cm^3 g^{-1}. No preferential orientation of the system with respect to the external field was imposed. Pulse sequence parameters are $\varepsilon = \pi/2$; $\Delta = 1.0$ ms, $t_1 = 30$ μs.

shown that in isotropic media the density matrix is a combination of only even ranked spherical spin tensors, while in aligned systems or in solid state odd rank tensors are created [25]. This observation has been exploited to distinguish by multiple-quantum filtering the free sodium from that interacting with aligned tissues in biological systems [25].

Double and triple quantum-filtered spectra are commonly measured using the pulse sequence

$$\pi/2\text{–}\Delta/2\text{–}\pi\text{–}\Delta/2\text{–}\epsilon\text{–}t_1\text{–}\epsilon\text{–}t_2(\mathrm{Acq}) \tag{15}$$

with $\varepsilon = \pi/2$. In the sequence, the first pulse transforms the equilibrium magnetization T_{01} (where the first subscript indicates the quantum jump and the second the rank) into single quantum T_{11}; no pulse can generate out of this tensor transitions of higher order than its rank but multiple quantum transitions are originated by relaxation phenomena acting during the delay Δ. Relaxation is able to transform T_{11} into T_{13} which, in turn, generates double and triple quantum transitions (T_{32} and T_{33}) under the effect of the second 90° pulse. The last 90° pulse makes the T_{33} and T_{32} tensors observable (by conversion into T_{11}). The conversion from T_{11} to T_{13} is easily understood looking at the equation (that can be calculated by the write equation routine) governing the relaxation of T_{11} tensor in the spherical tensors basis, which mixes the two terms:

$$\frac{\mathrm{d}(T_{11})}{\mathrm{d}t} = \left(\frac{e^2qQ}{4\hbar}\right)^2 \{T_{11}[10.8J(0) + 18J(\varpi) + 7.2J(2\varpi)] + T_{13}[8.8J(0) - 8.8J(2\varpi)]\} \tag{16}$$

or by the presence of a cross-term between these two elements of the relaxation matrix calculated in the same basis (Fig. 1).

Fig. 2 shows a plot generated by the program of T_{11}, T_{12}, and T_{13} as a function of the creation time Δ in aligned and isotropic media. The figure clearly shows that the double quantum tensor T_{12} is created only in the presence of alignment and thus DQF experiments can select sodium ions interacting with aligned tissues such as cartilage or DNA. As a consequence, DQF spec-

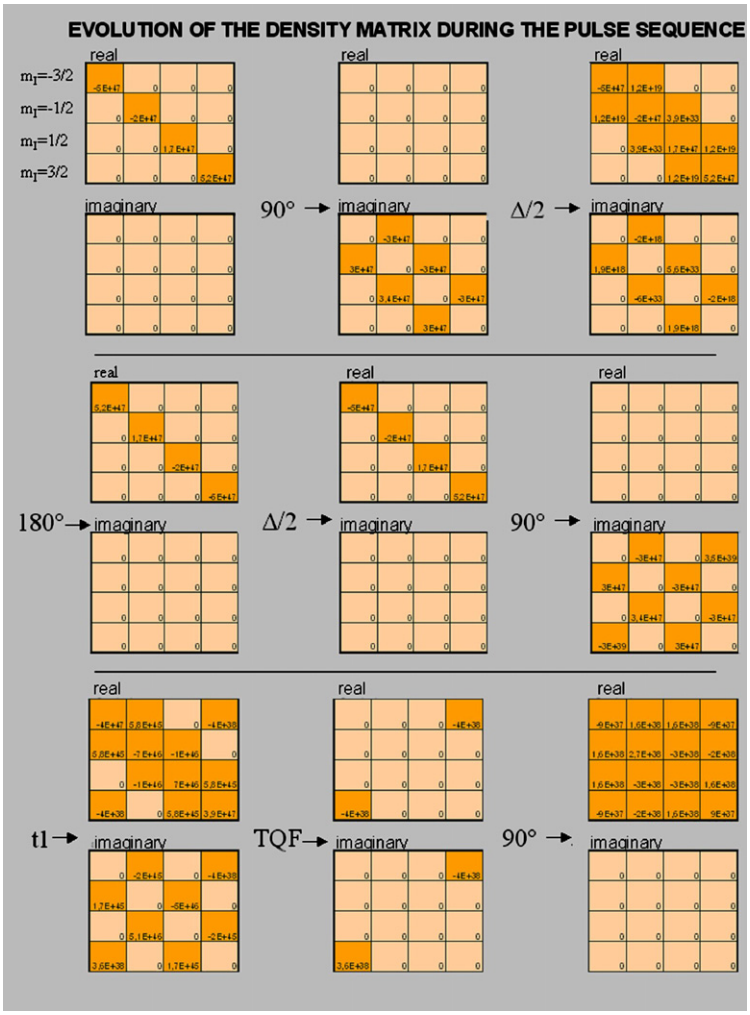

Fig. 5. Density matrix evolution under the effect of a MQF pulse sequence for slowly tumbling Na^+ ion. In each line, real (top) and imaginary (bottom) parts of the matrix are shown.

tra of aligned systems have contribution from both T_{12} and T_{13}, while TQF spectra have contribution from only T_{13}. This makes the shape of the resulting DQF spectrum dependent on the relative contribution of the two tensors (and thus on the creation time Δ, Fig. 3A) while the TQF spectrum only changes in amplitude at different Δ (Fig. 3B). Furthermore, it has been shown that using a value of 54.7° for ε eliminates the contribution from the third rank tensor [20,25,26] (Fig. 3C).

As the coherence creation is governed by relaxation, which in turn is modulated by the motion, slowly tumbling ions can be distinguished from fast tumbling ions and this observation has been exploited to distinguish between extra- and intracellular sodium in biological samples. Fig. 4A shows that the coherence transfer from T_{11} to T_{13} is more efficient for slowly tumbling systems (isotropically tumbling). Moreover, triple quantum filter is more sensitive to slowly tumbling sodium with respect to double quantum [27] as demonstrated by the comparison of the simulated spectra (Fig. 4B). The overall process can be visualized following the density matrix evolution (Fig. 5) in which it is clear that the initial magnetization (on the diagonal of the density matrix) is converted by the first pulse into single quantum magnetization (one space apart from the diagonal); the second 90° pulse generates double and triple quantum transitions (two and three spaces apart from the diagonal, respectively) to be selected by the filter, and the last pulse converts the filtered magnetization into the observable one.

3. Conclusions

We believe that this program can provide a useful user-friendly tool to understand the physical phenomena giving rise to the NMR spectrum of a quadrupolar nucleus. It can be used for planning the ideal conditions to set up specific new experiments or to give a physical interpretation of experimental results.

The Excel platform has the advantages of making the program easily exportable besides allowing the user to do personal modifications. The program was fully tested for Microsoft Visual Basic 6.0. Finally, we believe that the completely interactive interface makes it a useful tool also for educational purposes.

Acknowledgments

We thank Giovanni Della Lunga, Michela Pezzato, and Fabrizio Sicilia (Chemistry Department, University of Siena, Italy) for invaluable help in Excel programming and Moreno Lelli (CERM, University of Florence, Italy) for helpful discussions in the resolution of matrix algebra problems.

References

[1] R. Kemp-Harper, S.P. Brown, C.E. Hughes, P. Styles, S. Wimperis, ^{23}Na NMR methods for selective observation of sodium ions in ordered environments, Prog. NMR Spectr. 30 (1997) 157–181.
[2] M.E. Smith, E.R.H. van Eck, Recent advances in experimental solid state NMR methodology for half-integer spin quadrupolar nuclei, Prog. NMR Spectr. 34 (1999) 159–201.
[3] L.A. Jelicks, R.K. Gupta, Double-quantum NMR of sodium ions in cells and tissues. Paramagnetic quenching of extracellular coherence, J. Magn. Reson. 81 (1989) 586–592.
[4] A. Lehoux, M. Krzystyniak, E. Baguet, A faster way to characterize by triple-quantum-filtered ^{17}O NMR water molecules strongly bound to macromolecules in solution, J. Magn. Reson. 148 (2001) 11–22.
[5] T. Knubovets, H. Shinar, G. Navon, Quantification of the contribution of extracellular sodium to ^{23}Na multiple-quantum-filtered NMR spectra of suspensions of human red blood cells, J. Magn. Reson. 131 (1) (1998) 92–96.
[6] G. Navon, Complete elimination of extra-cellular ^{23}Na NMR signal in triple quantum filtered spectra of rat hearts in the presence of shift reagents, Magn. Res. Med. 30 (1993) 1–4.
[7] L. Tsoref, H. Shinar, Y. Seo, U. Eliav, G. Navon, Proton double-quantum filtered MRI. A new method for imaging ordered tissues, Magn. Res. Med. 40 (1998) 720–726.
[8] A. Abragam, The Principles of Nuclear Magnetism, Clarendon Press, Oxford, 1961.
[9] C.P. Slichter, Principles of Magnetic Resonance, Harper & Row, New York, 1963.
[10] J. Cavanagh, W.J. Fairbrother, A.G. Palmer III, N.J. Skelton, Protein NMR Spectroscopy: Principles and Practice, Academic Press, New York, 1996 (Chapter 5).
[11] M. Goldman, Quantum Description of High-resolution NMR in Liquids, Clarendon Press, New York, 1988.
[12] R.N. Zare, Angular momentum: understanding spatial aspects in chemistry and physics, Wiley, New York, 1988.
[13] R. Brüschweiler, D.A. Case, Characterization of biomolecular structure and dynamics by NMR cross relaxation, Prog. NMR Spectrosc. 26 (1994) 27–58.
[14] R.E. London, D.M. LeMaster, L.G. Werbelow, Unusual NMR multiplet structures of spin-1/2 nuclei coupled to spin-1 nuclei, J. Am. Chem. Soc. 116 (1994) 8400–8401.
[15] D.E. Woessner, Brownian motion and correlation times, in: D.M. Grant, R.K. Harris (Eds.), Encyclopedia of Nuclear Magnetic Resonance, 2, Wiley, New York, 1996, pp. 1068–1083.
[16] L.G. Werbelow, Relaxation theory for quadrupolar nuclei, in: D.M. Grant, R.K. Harris (Eds.), Encyclopedia of Nuclear Magnetic Resonance, 6, Wiley, New York, 1996, pp. 4092–4101.
[17] L.G. Werbelow, Dynamic frequency shift, in: D.M. Grant, R.K. Harris (Eds.), Encyclopedia of Nuclear Magnetic Resonance, Wiley, New York, 1996, pp. 1776–1783.
[18] C. Moler, C. Van Loan, Nineteen dubious ways to compute the exponential of a matrix, twenty-five years later, SIAM Rev. 45 (1) (2003) 3–49.
[19] Y. Sharf, U. Eliav, H. Shinar, G. Navon, Detection of anisotropy in cartilage using ^{2}H double-quantum-filtered NMR spectroscopy, J. Magn. Reson. B 107 (1995) 60–67.
[20] G. Jaccard, S. Wimperis, G. Bodenhausen, Multiple-quantum NMR spectroscopy of $S = 3/2$ spins in isotropic phase: a new probe for multiexponential relaxation, J. Chem. Phys. 85 (1986) 6282–6293.
[21] S. Vega, T.W. Shattuck, A. Pines, Fourier-transform double-quantum NMR in solids, Phys. Rev. Lett. 37 (1976) 43–46.

[22] J. Pekar, J.S. Leigh Jr., Detection of biexponential relaxation in sodium-23 facilitated by double-quantum filtering, J. Magn. Reson. 69 (1986) 582–584.
[23] N. Muller, Observation of multi-exponential longitudinal and transverse relaxation in two-dimensional NMR, Chem. Phys. Lett. 131 (1986) 218–223.
[24] L. Braunschweiler, G. Bodenhausen, R.R. Ernst, Analysis of networks of coupled spins by multiple quantum NMR, Mol. Phys. 48 (1983) 535–560.
[25] U. Eliav, H. Shinar, G. Navon, The formation of a second rank tensor in ^{23}Na double-quantum-filtered NMR as an indicator for order in a biological tissue, J. Magn. Reson. 98 (1992) 223–229.
[26] A. Allouche, G. Pouzard, L.G. Werbelow, Nuclear magnetic resonance flip-angle effects: observability of multipole operators. II, J. Chem. Phys. 82 (1985) 733.
[27] C.W. Chung, S. Wimperis, Optimum detection of spin-3/2 biexponential relaxation using multiple-quantum filtration techniques, J. Magn. Reson. 88 (1990) 440–447.